JOURNAL OF GEOPHYSICAL RESEARCH, VOL. 103, NO. B5, PAGES 10,141–10,160, MAY 10, 1998

Morphologic dating of scarps formed by repeated slip events along the San Andreas Fault, Carrizo Plain, California

J Ramón Arrowsmith

Department of Geology, Arizona State University, Tempe

Dallas D. Rhodes

Department of Geology, Whittier College, Whittier, California

David D. Pollard

Department of Geological and Environmental Sciences, Stanford University, Stanford, California

Abstract. Morphologic dating of fault scarps determines late Cenozoic fault activity by comparing observed topographic profiles with those determined using a calibrated hillslope development model. We postulate that the material transport rate along the profile is a function only of local slope and is transport-limited. Morphologic dating of hillslopes bounded by continuously dropping boundaries or cut by continuously slipping faults is used to determine the material transport rate constant, the time since the downdrop was initiated, or the fault began to slip. We calibrated the hillslope development model on the southwest facing scarp southeast of Wallace Creek along the San Andreas Fault (SAF) in the Carrizo Plain, California. The scarp has been exposed by right-lateral offset of a southeast sloping shutter ridge located on the southwest side of the SAF and by vertical offset related to secondary deformation. We assume that all the observed offset occurs after initial exposure of the scarp by passage of the shutter ridge. Forward modeling of profile development yielded a κ (mass diffusivity) of 8.6±0.8 m^2 kyr^{-1}. Normal fault slip rates were determined for two graben-bounding faults in the Northern Elkhorn Hills in the southeastern Carrizo Plain by applying the calibrated κ to the degradation of the scarps to determine the scarp age. One fault scarp began to form about 12 kyr ago and the other about 63 kyr ago. Those ages and estimates of the dip slip along the faults result in slip rates of 1-2 mm yr^{-1}.

1. Introduction

Dating late Quaternary fault activity at the Earth's surface depends primarily upon historic records or detailed microstratigraphic studies and direct dating of materials produced, deformed by, or bracketing surface rupture [e.g., *McCalpin*, 1996; *Yeats et al.*, 1997]. Studies of historic earthquakes may indicate the timing and occasionally the causative fault for earthquake ruptures up to about 2000 years ago [*Yeats*, 1994]. Trenching investigations may have temporal resolution of the order of a few tens of years over the last millennium [e.g., *Biasi and Weldon*, 1994; *McCalpin*, 1996; *Yeats et al.*, 1997]; however, they provide isolated data points at relatively large expense and there is much uncertainty regarding the linkages between the records from trenches separated by tens of kilometers.

Quantitative modeling of hillslope development may be sufficiently accurate for hillslopes to be dated by comparing observed profiles with model profiles determined from calibrated models ("morphologic dating" [e.g., *Hanks et al.*, 1984; *Nash*, 1986; *Avouac*, 1993]). The limitations of morphologic dating are that the types of processes controlling material transport over hillslopes are not well understood and their rates are not well known [e.g., *Colman*, 1987]. Nevertheless, where the processes may be identified and the rates calibrated, morphologic dating of faulted landforms provides broader temporal and spatial coverage than historic or trench investigations. For example, morphologic dating is limited temporally only by tectonic landform preservation, whereas the historic record is limited to periods of human occupation and record keeping, and the effective time limit of ^{14}C dating is less than 100 kyr and more likely 40 kyr [*Keller and Rockwell*, 1984; *Worsley*, 1990]. Furthermore, topographic profiles or maps (the basic data in morphologic dating) can be generated rapidly over broad areas using digital surveying or photogrammetric technology [*Kennie and Petrie*, 1990].

In this paper, we review a simple model for hillslope development to investigate the development of fault scarps and associated landforms. We use it predictively to obtain relative ages with confidence limits and to suggest absolute ages for fault scarps formed by strike-slip offset of topography and by repeated normal slip events along faults within the San Andreas Fault (SAF) zone in California. The application to specific scarps in California provides values for the transport

Paper number 98JB00505
0148-0227/98/98JB-00505$09.00

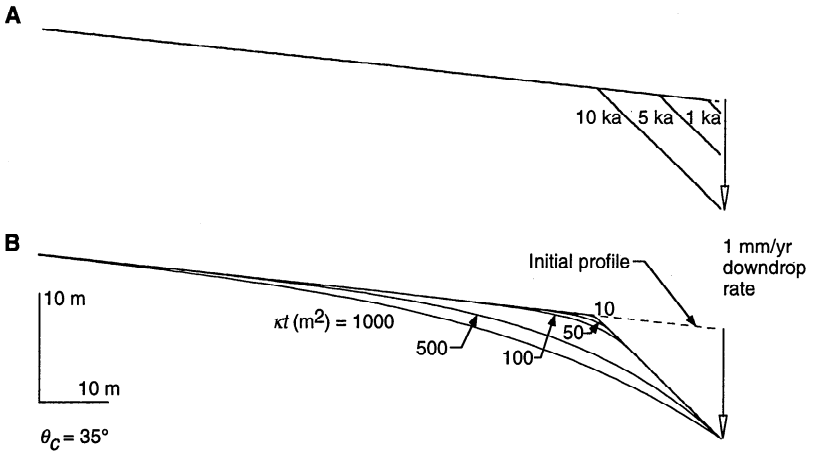

Figure 1. Examples of transport-limited topographic profile development subject to different transport processes. All material is removed from the system at the lower boundary, which drops at a constant rate. The upper boundary condition is constant elevation. The dashed line is the initial profile. (a) Profile development is controlled by threshold angle-dependent mass failure shown at different times (θ_c = 35°). (b) Diffusion erosion and critical angle for threshold angle-dependent mass failure (θ_c = 35°).

rate constant, slip rates and ages for scarps bounding grabens. The results raise interesting questions about the distributed deformation near the Big Bend of the SAF as well as provide insight into the processes controlling the development of tectonic landforms.

2. Transport-Limited Hillslope Development Model

The present approach to hillslope development follows the early work of *Culling* [1963], *Hirano* [1968], *Ahnert* [1970], *Kirkby* [1971], and *Carson and Kirkby* [1972]. It has been used in numerous geomorphic and tectonic applications investigating normal faulting and shoreline and terrace development [e.g., *Hirano*, 1968; *Nash*, 1980; *Hanks et al.*, 1984]. A more elaborate consideration of surface processes in areas of active tectonics is presented by *Arrowsmith* [1995] and *Arrowsmith et al.* [1996], where we considered surface wash (gullying) and weathering-limited conditions as well. We limit the analysis to changes in elevation $H(x,t)$ along a profile (x is the horizontal distance) over time, t (Figure 1). We assume that all material flows along the plane of the profile and that it maintains a constant density (a reasonable assumption for transport of unconsolidated, relatively fine-grained material). The determination of the vertical component of geomorphic displacement (erosion or deposition) is governed by the conservation of mass along the profile. Therefore we relate the material volume flow rate per unit width Q (with dimensions $[L^2T^{-1}]$) to the time rate of change of the vertical component of geomorphic displacement rate $\Delta V/\Delta t$ (erosion or deposition, with dimensions $[LT^{-1}]$) by applying the continuity equation to an infinitesimal slope element of length Δx [*Carson and Kirkby*, 1972; *Smith and Bretherton*, 1972; *Welty et al.*, 1984]:

$$\frac{\partial V}{\partial t} = -\frac{\partial Q}{\partial x}. \tag{1}$$

We assume that the conditions are always transport-limited. Thus we do not explicitly consider the conversion of bedrock to soil but assume either that it occurs at a rate greater than the erosion rate or that the material was never lithified.

The specification of boundary conditions strongly affects the model results and is a central problem in the calibration effort. Constant elevation, variable elevation, or constant material flux boundary conditions may exist in our model. A constant elevation boundary condition is easiest to imagine, although it is probably rare in nature. Typically, a profile boundary may be lowered or raised by tectonic or geomorphic processes operating beyond the landform of interest (i.e., a downdropping base level is important in the first part of our calibration study). A zero sediment flux upper boundary condition is used to simulate the lowering of a profile divide, and a zero sediment flux lower boundary is used to simulate deposition in a graben.

We consider mass failure as the relatively rapid flow of debris downslope and its settling at the angle of repose (θ_c). In our analysis, the angle of repose is specified, and greater slopes are immediately eroded and thus contribute to the material flux. This assertion of immediate mass failure is oversimplified. However, it provides a means of quickly reducing steep slopes to ones over which continuous processes regularly operate. Indeed, the reduction of steep scarps to ones at the angle of repose may occur in hundreds of years [e.g., *Wallace*, 1980; *Arrowsmith and Rhodes*, 1994], and the timescales of interest for fault scarp studies are typically in thousands of years. In the Carrizo Plain, there are no slopes above the angle of repose (i.e., free faces) that are preserved from the 1857 earthquake, the last to cause surface rupture there [*Sieh*, 1978]. Figure 1a illustrates the development of a slope with a continuously downdropping lower boundary, subject only to material transport by this process and with removal of the material at the base.

Along with immediate material transport over slopes above the angle of repose, we specify the rule for material transport as the following:

$$Q = -\kappa \frac{dH}{dx}, \tag{2}$$

where κ is a constant of proportionality (called diffusivity; with dimensions of $[L^2T^{-1}]$) and the negative sign is necessary for positive transport rate down a negative slope. This slope dependent law results from rain splash, creep, thermal expansion, and animal-induced disturbances [*Carson and*

Kirkby, 1972; *Culling*, 1963; *Selby*, 1985]. It does not allow for slope-length dependent processes (where Q is proportional to x), such as overland flow [*Carson and Kirkby*, 1972].

Combining (1) and (2) results in the following differential equation for the change in elevation with time (assuming transport-limited conditions with no tectonic displacements):

$$\frac{\partial H}{\partial t} = \frac{\partial V}{\partial t} = \kappa \frac{\partial^2 H}{\partial x^2}, \tag{3}$$

where the vertical geomorphic displacement rate is proportional to the curvature of the landscape.

In summary, for this paper we limit the modeling to the representative processes illustrated in Figure 1: mass failure (Figure 1a) in combination with processes for which the material transport is directly and linearly proportional to the local slope only (Figure 1b). The latter is a condition of "diffusion erosion" and produces a convex profile under the conditions of a constant base level drop. Equation (3) is solved numerically for a given initial profile, boundary conditions, landform age, and tectonic displacement history using a finite difference approach [e.g., *Arrowsmith*, 1995; *Arrowsmith et al.*, 1996]. A major hypothesis is that if the recurrence time for events that displace the surface is short compared to the age of the landform, a constant baselevel drop or constant slip boundary condition may be used.

3. Morphologic Dating

The development of the final profile form depends upon the passage of time t and the value of the rate term, κ. It is the product of these two parameters (called the morphologic age κt) that uniquely defines the form. We assume that κ is not a function of time, space, or material and only applies to the diffusive slope processes. Such an assumption is not justified in general. However, we discuss its justification below for the specific calibration of this paper. Small t and large κ define the same form as large t and small κ [*Hanks et al.*, 1984; *Hanks*, 1997]. Therefore, in the calibration, we determine the best fitting κt and use knowledge of t determined in trenching investigations by other researchers to first determine κ. Then we use the calibrated κ to determine t and thus the age of fault scarps elsewhere and possibly the slip rate for faults of interest.

4. Calibration, Forward Modeling, and Model Misfit

In order to determine the best fitting values of κt for the different processes, we choose the representative profiles, estimate the initial shape and boundary conditions, and then by forward numerical modeling perform a parameter search in which κt is incremented, and for each value the modeled and observed profiles are compared and the root mean square of the misfit between observed and modeled profiles is determined [*Avouac*, 1993; *Bevington and Robinson*, 1992; *Kirkby et al.*, 1993].

$$\mathrm{RMS} = \left\{ \frac{1}{p} \sum_{i=1}^{p} \left[H_i - H_{\mathrm{model}}(x_i) \right]^2 \right\}^{1/2}, \tag{4}$$

where p is the number of observations defining the profile, H_i is the elevation at distance x_i along the profile from the divide, and $H_{\mathrm{model}}(x_i)$ is the model elevation at x_i (*Avouac* [1993] refers to this as standard deviation). The distribution of

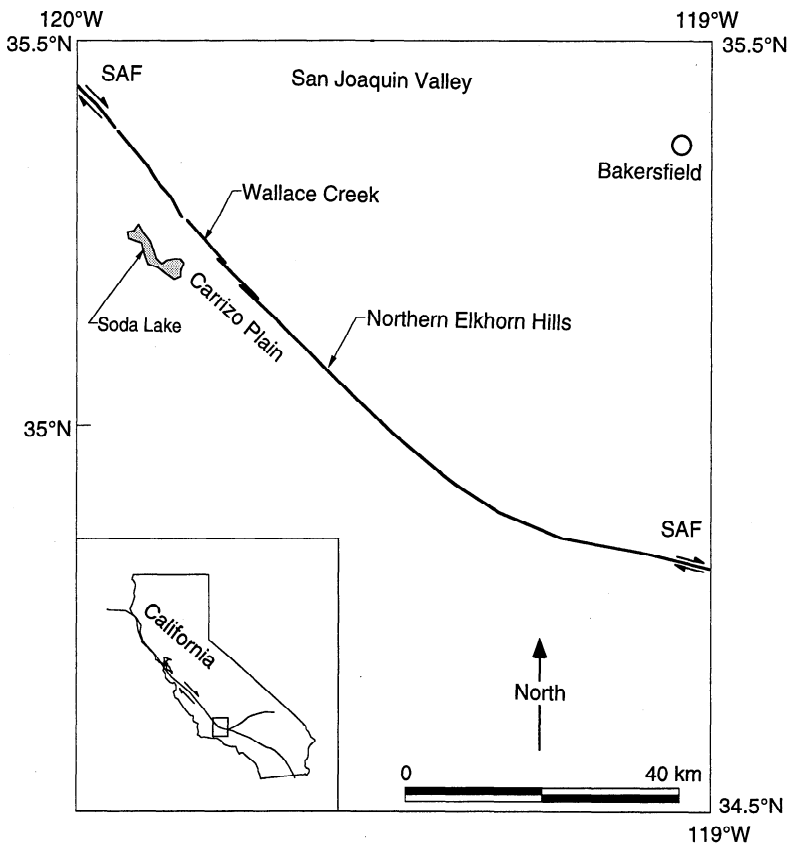

Figure 2. Index map of central California showing the location of the Carrizo Plain and the location of the study areas (Wallace Creek and the Northern Elkhorn Hills). Soda Lake may preserve the climate record for the region.

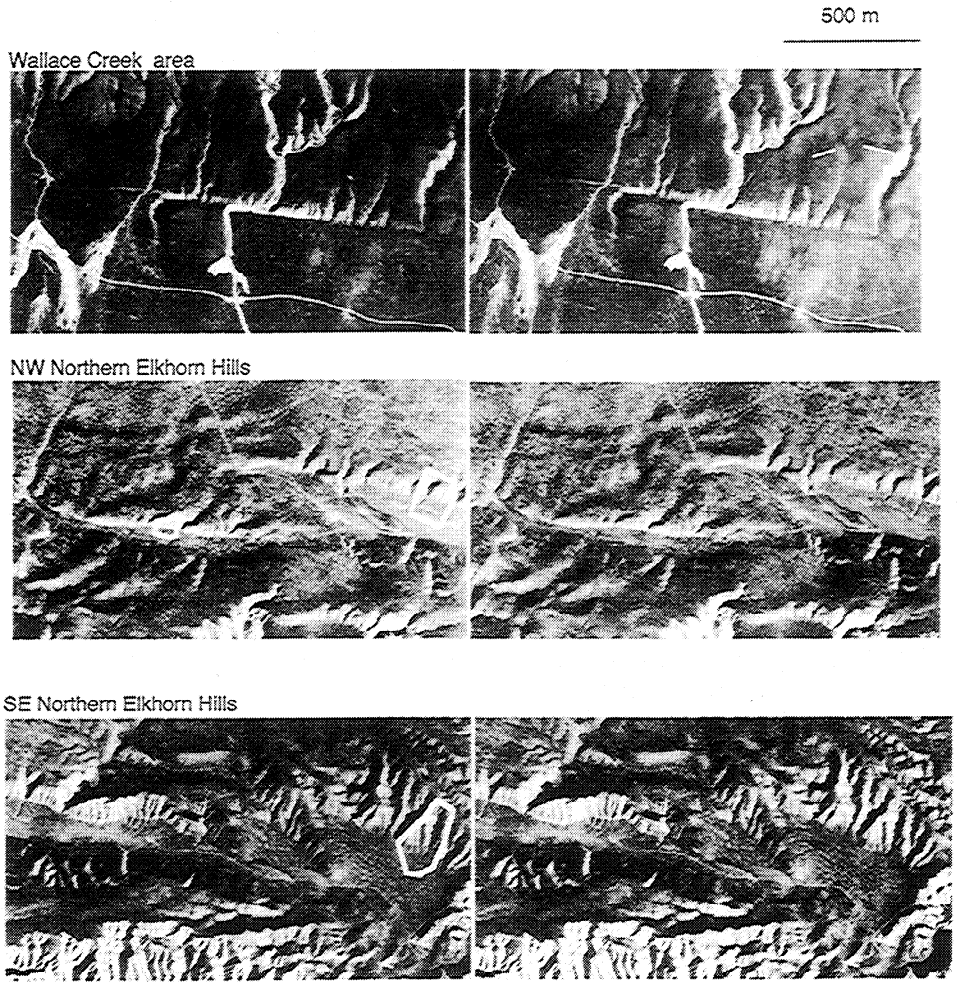

Figure 3. Stereo aerial photographs of the study areas: Wallace Creek and the Northern Elkhorn Hills. The NW edge of the topographic welt near Wallace Creek is shown on the upper right with white lines along its crest. The white polygons in the Elkhorn Hills photographs outline the topographic maps in figure 9. The scale is the same for all the images. Aerial photography is courtesy of the Fairchild Aerial Photography Collection at Whittier College. The original photographic scale was 1:24,000 (flight C-3883 on February 27, 1936).

RMS versus κt usually passes through a well-defined minimum (RMS_{min}), which defines the best fitting model profile at κt_{min} [*Avouac*, 1993]. We define confidence intervals on the best fitting value by considering all profiles that fit the observations within a specified RMS range of RMS_{min} (in this study and that of *Avouac* [1993] and *Avouac and Peltzer* [1993], it is 5 cm; we discuss this choice in section 7).

The summary value (for all individual profile fits) of κ_μ $\pm\Delta\kappa_\mu$ is computed in the following way. The value κ_μ is the weighted mean,

$$\kappa_\mu = \frac{\sum_{j=1}^{n} \left(\kappa_j / \Delta\kappa_j^2\right)}{\sum_{j=1}^{n} \left(1/\Delta\kappa_j^2\right)}, \quad (5)$$

in which n is the number of individual determinations κ_j and where each is weighted inversely by its own variance $\Delta\kappa_j^2$ in the sum. The uncertainty of the mean, $\pm\Delta\kappa_\mu$, is determined by

$$\Delta\kappa_\mu^2 = \frac{1}{\sum_{j=1}^{n} \left(1/\Delta\kappa_j^2\right)} \quad (6)$$

[*Bevington and Robinson*, 1992].

5. Model Calibration

We have chosen the tectonic landforms along the SAF zone in the Carrizo Plain of California (Figure 2) as the subject of our calibration experiment. Figure 3 shows stereo aerial photographs of the specific study areas. The late Quaternary geologic history of many tectonic landforms in the Carrizo Plain has been well studied [e.g., *Wallace*, 1968; *Sieh and Jahns*, 1984; *Sieh and Wallace*, 1987]. In our related work investigating the active tectonic deformation along this portion of the San Andreas Fault (SAF) zone in the transition from a straight to a restraining strike-slip fault segment (see section 9 and *Arrowsmith* [1995]), we use the slip rates determined in this study as input for mechanical analysis of the deforming fault zone over tens of kiloyears.

6. Rate Constant Calibration

6.1. Wallace Creek Geologic and Geomorphologic Background

The north central Carrizo Plain area preserves some of the most well-developed strike-slip offset channel complexes in

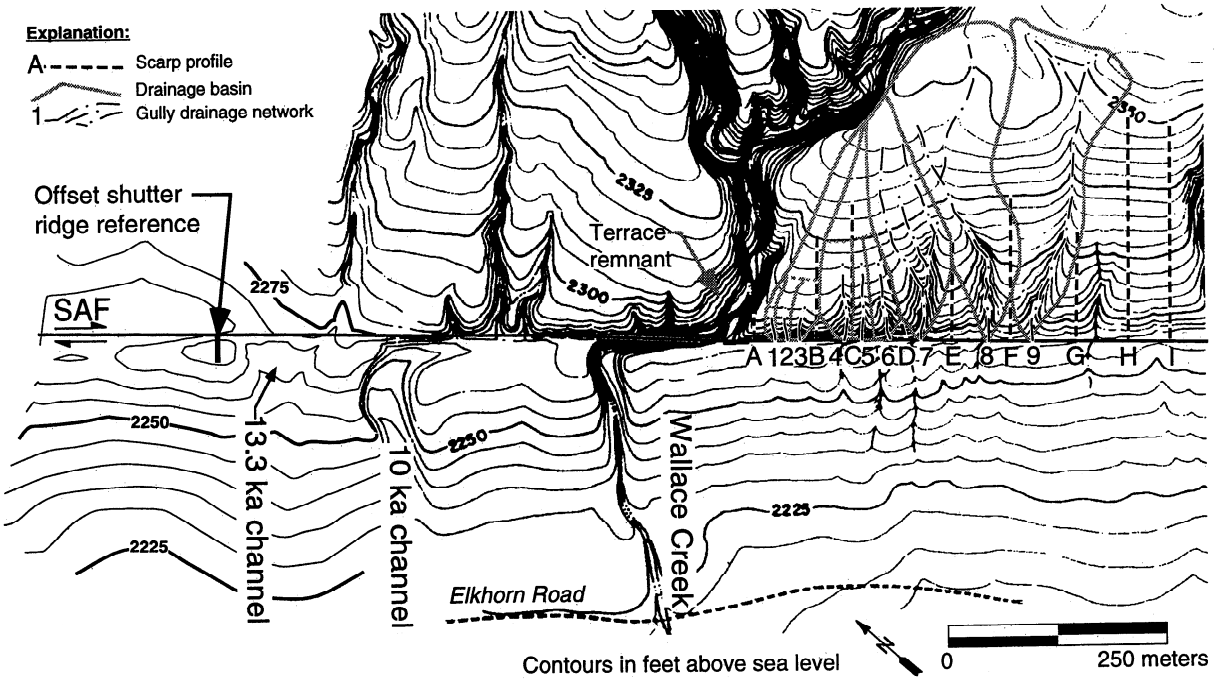

Figure 4. Topography and selected landforms around Wallace Creek. Topography southeast of the 10 kyr channel is from *Sieh and Wallace* [1987]. Data surveyed in this study define the topography in the northwest portion of the map. The locations of the landforms investigated in this study as well as those defined by *Sieh and Jahns* [1984] are shown.

the world. One of these complexes, Wallace Creek, has been the subject of intensive investigation [*Wallace*, 1968, 1975; *Sieh and Jahns*, 1984; *Sieh and Wallace*, 1987]. At this site, the SAF cuts through a late Pleistocene alluvial fan complex and offsets gullies formed at the SAF and drainages crossing it flowing from the Temblor Range to the closed depression at the center of the Carrizo Plain (Figures 2, 3, and 4). *Wallace* [1968] suggested a chronology of offset and abandonment that was elaborated and corroborated in a detailed geomorphic and trenching investigation by *Sieh and Jahns* [1984] (see Figures 4 and 5):

1. The late Pleistocene fan material ("older fan alluvium" of *Sieh and Jahns* [1984], underlying all other units exposed at the site and derived from the Temblor Range to the NE), was deposited relatively continuously as thin sheets, lenses, and stringers of indurated silty clay, pebbly sandy clay, and sandy gravel. Charcoal disseminated within this unit about 4 m below the present fan surface yielded an age of 19,340±1000 years B.P. (all radiocarbon ages were corrected for isotopic fractionation and are in calendric years B.P. [*Sieh and Jahns*, 1984]). The lack of small channels indicates that any scarps formed during this time were less than 1 m high or faced NE, ponding material [*Sieh and Jahns*, 1984]. The age of the charcoal provides a maximum age for the end of deposition of the older fan alluvium (see the "X" on Figure 5b for the location of this deposit).

2. About 13 kyr ago, the entrenchment of the older fan alluvium occurred as several small gullies (7, 8, 9, and the gully between scarp profiles G and H on Figure 4 which are denoted as A, B, C, and D by *Sieh and Jahns* [1984]) eroded into the exposed older fan alluvium. The debris was deposited as the "younger fan alluvium" of *Sieh and Jahns* [1984], Py on Figure 5c. The material immediately below the base of the younger fan alluvium gave an age of 13,250±1650 years B.P. At about this time, the entrenchment of Wallace Creek began (13.3 kyr channel on Figure 4 and first paleochannel on Figure 5).

3. After the first paleochannel was offset about 100 m, it was abandoned, and the second paleochannel was incised (about 10 kyr ago; Figure 5d).

4. Within the channel of Wallace Creek, several terrace remnants are preserved (Figure 4). They are underlain by the "high channel alluvium" of *Sieh and Jahns* [1984]. This predominantly massive and poorly sorted material may have been deposited by debris flows in Wallace Creek when its bed was at a higher level until about 3680±155 years B.P. Southwest of the SAF, the upper end of the offset portion of the now abandoned second paleochannel is filled by channel deposits overlain by colluvium. These deposits yielded an age of 3780±155 years B.P. and are correlated with the high channel alluvium [*Sieh and Jahns*, 1984]. Thus, at about 3800 years B.P., the second paleochannel was abandoned and the modern channel of Wallace Creek incised (Figure 5e and the modern Wallace Creek landscape in Figure 4).

The late Quaternary geomorphic and geologic development of the Wallace Creek offset channel complex and important landforms and surfaces are shown in Figure 5. This illustrates the reconstruction of the lateral offset and the initial topography and not the development of the topography nor the vertical displacements due to localized deformation (see section 6.3). The inferred initial topographic surface is shown northeast of the SAF. It is not completely incised in the upper portions of the study area. It is possible to identify the surface in the field and on aerial photographs. Representative points and their elevations define the surface. It has been incised by the larger drainages, and near the SAF it has been eroded by the

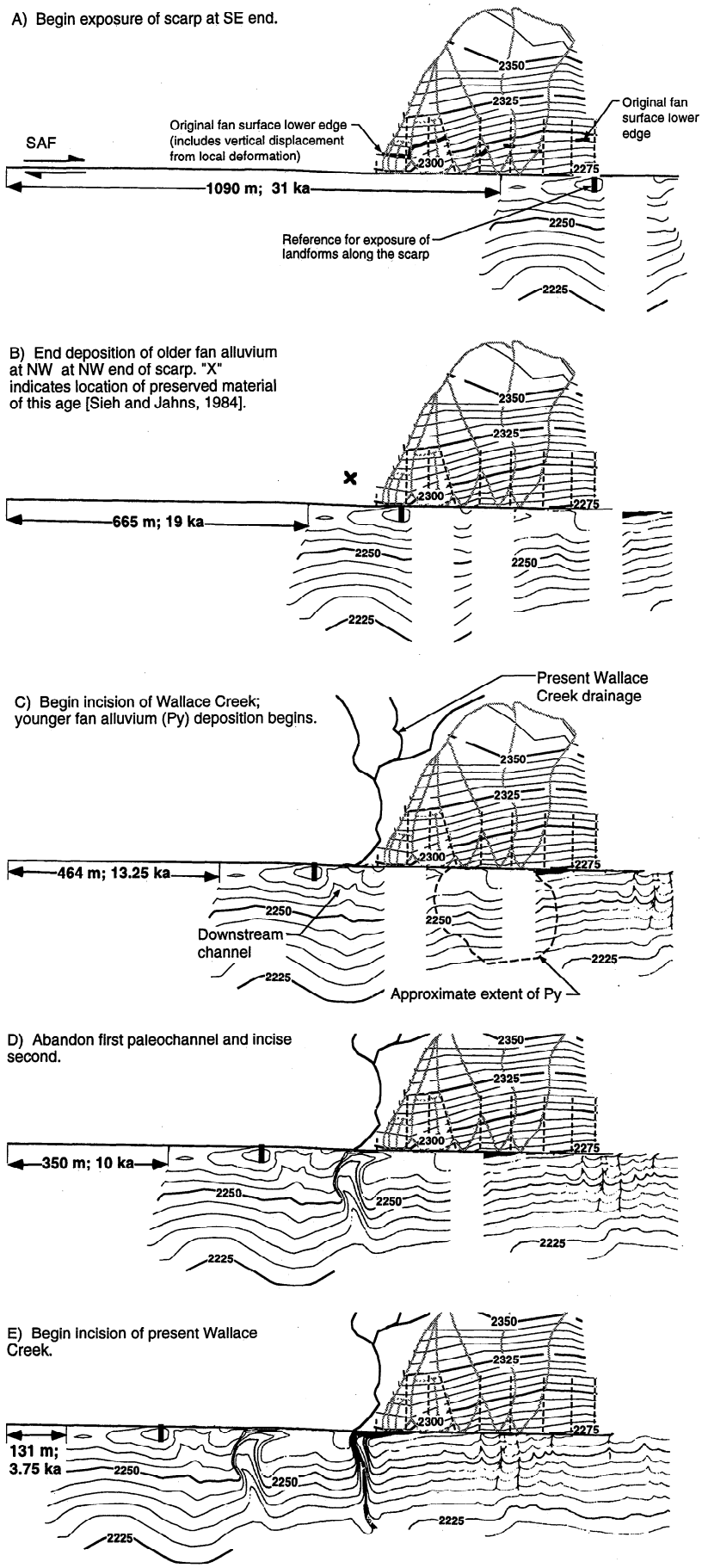
A) Begin exposure of scarp at SE end.
SAF
Original fan surface lower edge (includes vertical displacement from local deformation)
Original fan surface lower edge
1090 m; 31 ka
Reference for exposure of landforms along the scarp
2350
2325
2300
2275
2250
2225
B) End deposition of older fan alluvium at NW at NW end of scarp. "X" indicates location of preserved material of this age [Sieh and Jahns, 1984].
665 m; 19 ka
C) Begin incision of Wallace Creek; younger fan alluvium (Py) deposition begins.
Present Wallace Creek drainage
464 m; 13.25 ka
Downstream channel
Approximate extent of Py
D) Abandon first paleochannel and incise second.
350 m; 10 ka
E) Begin incision of present Wallace Creek.
131 m; 3.75 ka

small drainages and the diffusive and mass failure processes. The edge of the surface is shown as bold lines in Figure 5a. In the area where the surface has been completely removed, we inferred its initial location by projecting the existing surface at a constant slope to its intersection with the SAF. This surface is used to determine the initial forms of the scarp profiles that we analyzed.

6.2. Reconstruction of the Progressive Exposure of the Scarp Southeast of Wallace Creek

In order to determine a possible exposure time for the different landforms along the scarp, we held the northeast (upper) block fixed, assuming a constant strike-slip rate of 35 mm yr^{-1}, and laterally offset the topography on the southwest side starting at the inferred time of exposure of the southeastern limit of the study area (Figure 5a).

We assume that the incision of the fan surface was controlled by the passage of the high point of the shutter ridge marked with a vertical bar on Figures 4 and 5. This assumption is supported by the reconstruction. First, it addresses the apparently progressive exposure and development of the landforms along the scarp suggested by the degree of rounding and diminished slope of the ungullied portions of the scarp and by the degree of drainage development of the gullies. Second, the southwest side down vertical separation across the SAF may have initiated the incision of Wallace Creek at 13.3 kyr ago, and we note that the first paleochannel is just southeast of the shutter ridge high, consistent with exposure following passage of the shutter ridge (Figures 4 and 5c). Apparently, that incision was rapid because Wallace Creek had an established drainage basin with flow originating in the Temblor Range. The lag in large-scale deposition of Py after the initiation of the scarp-draining gullies may be attributed to the time required for the drainage systems to develop (~7 kyr from exposure by passage of the shutter ridge to gully initiation and development as indicated by the deposition of Py at 13.3 kyr ago). Finally, Figure 5b shows that the scarp near modern Wallace Creek was not exposed at 19 kyr ago; the charcoal deposit that yielded the 19 kyr age for older fan alluvium age comes from a trench on the NW side of the modern Wallace Creek channel (see "X" on Figure 5b), an area that may have been accumulating fan deposits while the scarp to the SE was being incised.

We do not think that the scarp was exposed in a single event (it would require a vertical offset of ~10 m along a segment of the SAF that has demonstrated evidence for large magnitude horizontal offsets only). Another hypothesis for the exposure is that variable vertical offsets not due to the offset of topography have accumulated since 13.3 kyr ago. However, the arguments presented above for the progressive exposure are compelling, so our preferred exposure history includes both the lateral offset of the SW block with exposure as the shutter ridge passes by and the variable offset apparently caused by local deformation. The vertical separation rate due to the lateral offset of the SW block is 0.16 mm yr^{-1}. It is determined by taking the height difference between shutter ridge top (692 m) and the current elevation at the SE end of study area (687 m) and dividing by the apparent time of exposure at the SE end of study area (31 kyr ago). The age of exposure is determined by dividing the distance between the shutter ridge top and the SE end of the study area (1090 m) by the strike-slip rate of 35 mm yr^{-1} (Figure 5a).

6.3. Northeast-Side-Up Vertical Offset Along the SAF at Wallace Creek

Vertical offset must be localized near the present junction of Wallace Creek and the SAF. In Figure 6, we plot the inferred vertical separation determined by subtracting the present elevation at the SAF from the inferred initial elevation, the contoured surface in Figure 5a shown in Figure 6 with circles. The total vertical separation at the lower end of these landforms varies from about 3.8 m to over 10 m. Up to 4.6 m can be attributed to the lateral offset of the shutter ridge and southeast sloping surface along the SAF (straight line), but that amount decreases to the NW. Subtracting the amount due to lateral offset of topography from the total leaves the residual, which indicates an anomalous vertical offset concentration along the SAF, with a maximum at about the location of profile B (dashed line on Figure 6). The local increase in vertical offset also may have deformed the high channel terrace surface (as suggested by *Sieh and Jahns* [1984], see their Figure 5). The height difference between the terrace and the modern channel is greatest at the SAF and the two merge about 1 km upstream. Judging from the elevation difference between the high terrace remnant and its correlative deposits across the SAF in the upper end of the second paleochannel (10 kyr channel on Figure 4), *Sieh and Jahns* [1984] concluded that the vertical offset over the past 3800 years was 3 m (0.8 mm yr^{-1}). They suggested that within 1 km to the northwest and southeast, the vertical offset diminished to zero and reversed sense. If our inferences for the exposure ages for the landforms along the scarp are reasonable, the missing vertical offset rate is <0.4 mm yr^{-1} (i.e., profile B was exposed 18.9 kyr ago by passage of the shutter ridge and we

Figure 5. (opposite) Reconstruction of offset and the initial topography along the scarp southeast of Wallace Creek. (a) Beginning of exposure of scarp at SE end. (b) Ending of deposition of older fan alluvium at NW end of scarp. (c) Beginning incision of Wallace Creek. (d) Abandoning of first paleochannel and incising of second. (e) Beginning incision of present Wallace Creek. The inferred initial topographic surface is shown above (NE) the SAF. This surface is not completely incised in the upper portion of the study area. Below the lower edge of this fan surface (bold lines), the original surface was reconstructed by projecting the surface at a constant slope to the SAF. Much of the topography is removed to simplify the diagram and the drainage of Wallace Creek are obscured until it is inferred to have developed. We use a long term average strike-slip rate of 35 mm yr^{-1} [*Sieh and Jahns*, 1984] to offset the topography. We do not account for the vertical displacements due to localized deformation immediately southeast of Wallace Creek. The vertical bar at the highest point on top of the shutter ridge on the southwest side of the SAF is used as a reference. We assume that its passage exposes the northeast block. Note that the modern Wallace Creek landscape is shown in Figure 4. The drainage basin outlines and the scarp profiles are shown as in Figure 4.

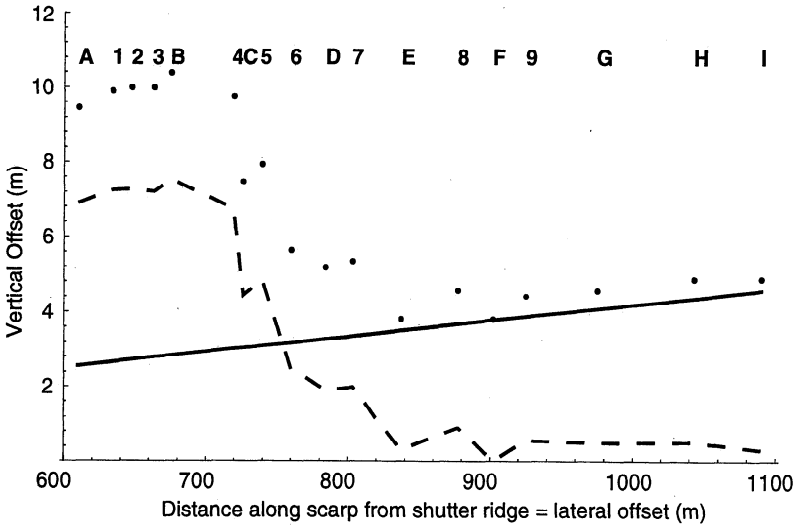

Figure 6. Plot of inferred total vertical offset (in meters, as circles) for each landform (scarps indicated by letters and gullies indicated by numbers, see Figure 4 for locations) with distance along the scarp (meters). The solid line shows the amount of vertical separation due to the lateral offset of the gently southeast sloping surface (on the southwest side of the SAF), assuming exposure of the landforms by lateral offset of the shutter ridge. The dashed line shows the residual vertical offset, possibly caused by local deformation. The residual vertical offset is determined by subtracting the two other curves and illustrates that the secondary deformation is localized in the area from scarp profile E to the northwest.

assume that the residual vertical offset of 8.4 m accumulated since then also).

A sinuous hill, a few meters to a few tens of meters high striking parallel to the SAF about 300 - 500 m NE of the SAF, has one end that terminates in the area of the uplifted fan surface SE of Wallace Creek (see the white lines along its crest in the upper right of Figure 3; it appears as a ridge in the east corner of Figure 4; it is also evident in the frontispiece of *Wallace* [1990]). From its NW termination, it is ~4 km long to the SE. The edges of the hill are sharpest along its NW end (nearest Wallace Creek) and may indicate its relatively more recent or rapid formation there. K. E. Sieh (personal communication, 1990 and 1994) suggested that this topographic welt may overlie a shallow thrust fault. We have observed a small normal fault in one of the gullies that cross it. In the Elkhorn Hills (Figures 2 and 3), we have mapped many folds and suggested that a shallow thrust fault dips back toward the SAF [*Arrowsmith*, 1995], but other evidence for thrusting in the area near Wallace Creek has not been forthcoming. For this study, we conclude that some deformation source, possibly uplift near the termination of a shallow thrust fault, has produced up to 8.6 m of vertical offset, NE side up, along the SAF centered just SE of Wallace Creek. We also assume that all of the vertical offset has accumulated since the passage of the shutter ridge marked with the vertical bar on Figures 4 and 5, consistent with the reconstruction presented above.

6.4. Rock Type and Material Supply

For conditions to be transport limited, the material must be effectively unconsolidated. The Pleistocene Paso Robles Formation and the Holocene alluvial fan units which underlie much of the Carrizo Plain and Elkhorn Hills are poorly consolidated [*Galehouse*, 1967; *Vedder*, 1970; *Dibblee*, 1973; *Sieh and Jahns*, 1984]. They are generally moderately sorted, medium sands with occasional pebble to cobble stringers. The material transport over these surfaces is influenced significantly by animal burrowing (see sections 2 and 7 and *Wallace* [1991]). The bioturbation appears to provide adequate supply of material for transport. Furthermore, the Paso Robles Formation retains a fairly uniform sedimentologic character over the spatial scales of our study area. Therefore we consider material differences to be of low significance.

6.5. Climate

Variations in climate affect the precipitation, storm magnitude, duration and occurrence, and temperatures and therefore must affect transport rates. Our approach to the effects of such variations in the transport rates is to assume that all scarps of similar age will have experienced the same average climate. Furthermore, all of the Carrizo Plain scarps investigated have similar aspect, and therefore microclimatic effects can be ignored [*Pierce and Colman*, 1986]. The degree and temporal distribution of climate variation over the late Quaternary in the Carrizo Plain is not well constrained in light of current data. We have not observed any shoreline terraces or other features that would indicate large volumes of standing water in Soda Lake (Figure 2), so that Pleistocene moisture may not have been significantly different from that of the present. If climatic variations are not significant, the lack of large variations in Pleistocene glacial-interglacial climate at these latitudes may be corroborated [*Porter*, 1989] and thus disregarded subsequently (see also the discussion by *Rosenbloom and Anderson* [1994, p. 14,017]).

6.6. Initial and Final Profiles

Along with the total vertical offset of the base of the landforms, we determined an initial profile from the inferred surface contour map of Figure 5. The final topographic

Table 1. Summary of Morphologic Dating (Diffusion Erosion) at the Wallace Creek Study Area

Profile	Offset Distance,[a] m	Age,[b] kyr	Determined Graphically: Minimum age, kyr	Maximum age, kyr	Minimum RMS,[c] m	Best κt, m^2	$-\Delta \kappa t$, m^2	$+\Delta \kappa t$, m^2	$\pm\Delta \kappa t$, m^2	κ,[d] m^2 kyr^{-1}	$\pm\Delta \kappa$,[d] m^2 kyr^{-1}	Uncertainty in the SAF slip rate: Minimum κ,[e] m^2 kyr^{-1}	Maximum κ,[e] m^2 kyr^{-1}	$-\Delta \kappa$,[f] m^2 kyr^{-1}	$+\Delta \kappa$,[f] m^2 kyr^{-1}	$\pm\Delta \kappa$,[f] m^2 kyr^{-1}	Graphical Uncertainty - Slip Rate Uncertainty[g] m^2 kyr^{-1}
A	610	17.0	14.8	19.2	0.11	179	24	25	25	10.5	1.5	9.3	12.1	1.2	1.6	1.6	-0.1
B	675	18.9	16.4	21.3	0.14	151	23	24	24	8.0	1.3	7.1	9.2	0.9	1.2	1.2	0.1
C	726	20.3	17.6	22.9	0.33	325	77	97	97	16.0	4.8	14.2	18.5	1.8	2.5	2.5	2.3
D	784	21.9	19.0	24.7	0.17	115	31	34	34	5.3	1.6	4.7	6.1	0.6	0.8	0.8	0.8
E	837	23.4	20.3	26.4	0.17	152	42	50	50	6.5	2.1	5.8	7.5	0.7	1.0	1.0	1.1
F	902	25.2	21.9	28.5	0.23	353	102	123	123	14.0	4.9	12.4	16.1	1.6	2.1	2.1	2.8
G	975	27.2	23.7	30.8	0.28	530	133	159	159	19.5	5.8	17.2	22.4	2.3	2.9	2.9	3.0
H	1043	29.1	25.3	32.9	0.23	553	176	285	285	19.0	9.8	16.8	21.9	2.2	2.9	2.9	6.9
I	1090	30.4	26.5	34.4	0.18	592	169	212	212	19.5	7.0	17.2	22.3	2.3	2.9	2.9	4.1
Summary for all profiles[h]										8.6	0.75						

See Figure 4 for locations of the landforms, see Figure 7 for individual profile investigations, and see Figure 8 for a summary plot of the parameter values. See text for discussion of Table 1.

[a]Distance southeast along the SAF from the shutter ridge crest (Figures 4 and 5).

[b]Age is the offset distance divided by the slip rate (35.8 mm yr^{-1}). Minimum age is the offset distance divided by the maximum slip rate [(35.8+5.4) mm yr^{-1}]; and the maximum age is the offset distance divided by the minimum slip rate [(35.8-4.1) mm yr^{-1}]. Slip rate is from *Sieh and Jahns* [1984].

[c]The minimum RMS is at the best fitting κt value (see equation (4) and Figure 7).

[d]These are determined by dividing the best κt or $\pm\Delta\kappa t$ value by the age. The uncertainty in the age is included in the graphical parameter determination.

[e]The minimum and maximum κ due to uncertainty only in the SAF slip rate are determined by dividing the best morphologic age (κt) by the maximum and minimum age (columns 5 and 4), respectively.

[f]The uncertainties are the differences between κ and the maximum and minimum values due to SAF slip rate uncertainty determined according to footnote e. The $\pm\Delta\kappa$ value is the maximum of the plus or minus uncertainty (in this case always equal to the plus uncertainty).

[g]The difference between the uncertainty in the κ value due to the SAF slip rate uncertainty and that due to the graphical determination indicates that the 5 cm minimum RMS can generally account for the uncertainty due to the slip rate.

[h]The summary value is a mean of the individual determinations weighted inversely by their variance (see equations (5) and (6)).

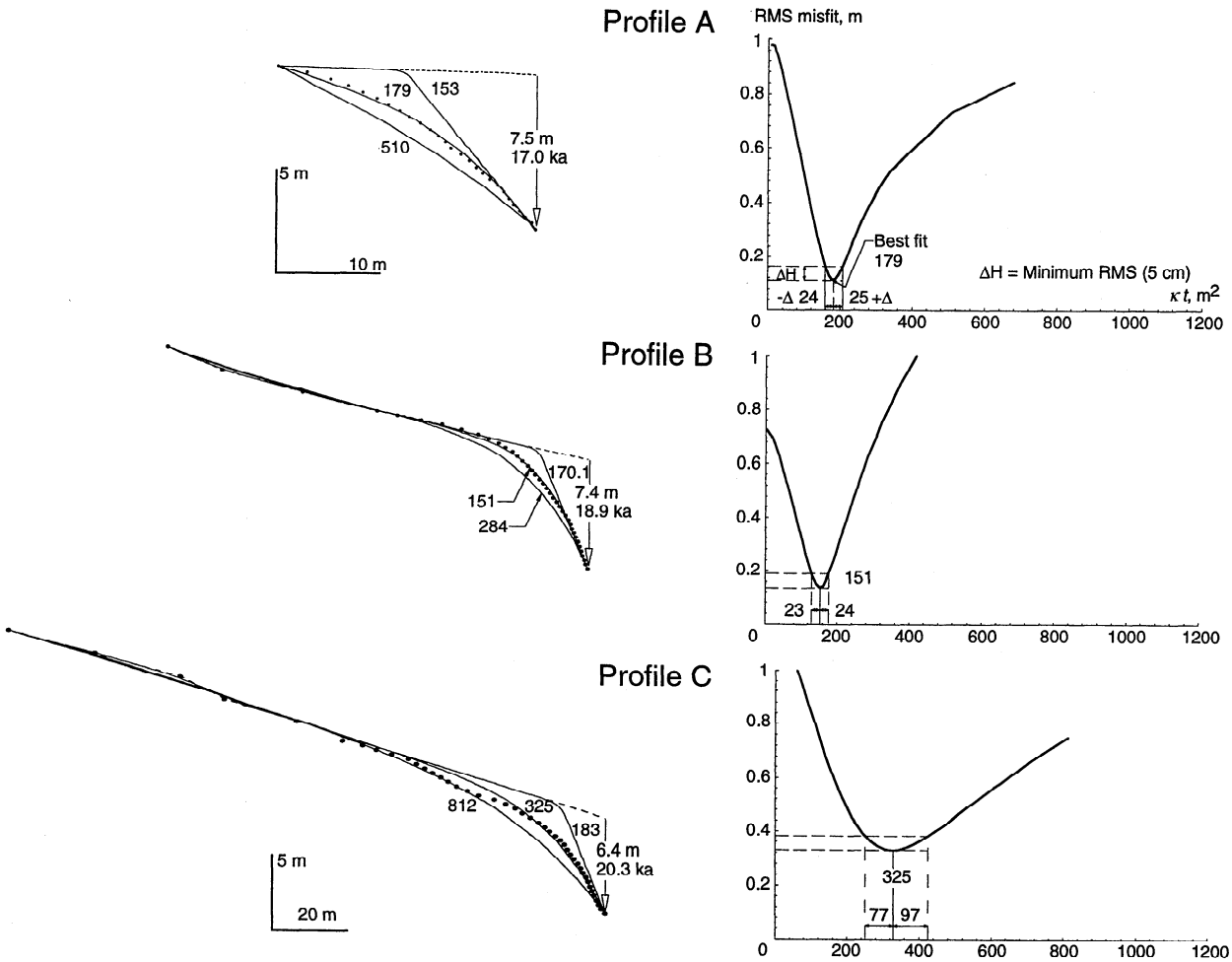

Figure 7. Summary of κt parameter search on Wallace Creek fault scarp profiles. The left column shows the observed profile (circles), model profiles (the best fitting one and representative bracketing examples, the numbers are the corresponding κt values), the initial profile (dashed line), and the vertical offset magnitude and time to accumulate the offset. The scale bars apply to profiles adjacent and above to the next scale bars. The right-hand column shows the corresponding plot of RMS misfit versus parameter value. The features of the graphical determination of uncertainty are labeled for profile A. The graphical determinations are summarized in Table 1, and the RMS versus morphologic age curves are investigated in the appendix. Note the horizontal and vertical scales for the profiles, and the variation in the scale for the morphologic age between profiles A-F and G-I.

profiles for comparison with model results use data from a detailed 0.3 m contour interval topographic and geomorphic strip map parallel to and spanning the SAF by 100 m [K.E. Sieh and R.H. Jahns, unpublished map, 1977]. These detailed data were supplemented by topographic data from the 1.5 m contour interval map shown in Figure 4 [*Sieh and Wallace*, 1987].

7. Calibration of κ at Wallace Creek

Much of the material transport on the hillslopes in the Carrizo Plain is (and may have been) accomplished by burrowing animals. This process may be considered diffusive [*Rosenbloom and Anderson*, 1994; *Selby*, 1982; 1985]. We selected nine scarp profiles (lettered on Figure 4) for calibration of κ. In this paper, we do not present the results from morphological modeling of the gullies which were promising but inconsistent [*Arrowsmith*, 1995]. The results for κ are shown in Figure 7 and tabulated in Table 1, and the parameter values are summarized in Figure 8. All model runs were made using a spatial step size of 0.5 m to ensure that the mass failure portion of our analysis resolved the details of the geomorphic responses to the steep slopes at the boundary. Constant elevation upper boundary conditions were prescribed, and the lower boundary dropped at a constant rate over the model run time to accumulate the total vertical offset (the difference between the elevation of the lower end of the initial and final profiles, note the vertical arrows in Figure 7). No other tectonic displacements are applied to the profile. We assume that there is no dextral shear within the NE block over which the profiles are made. We assume that all material is removed from the system at the lower boundary (the plane of the SAF). Thus, from the point of view of the profiles, the problem becomes one of continuously downdropping base level.

The model scarp profiles have more data in their lower and steeper portions because of the localized coverage of the 0.3 m contour map (Figure 7). This is an advantage because the RMS

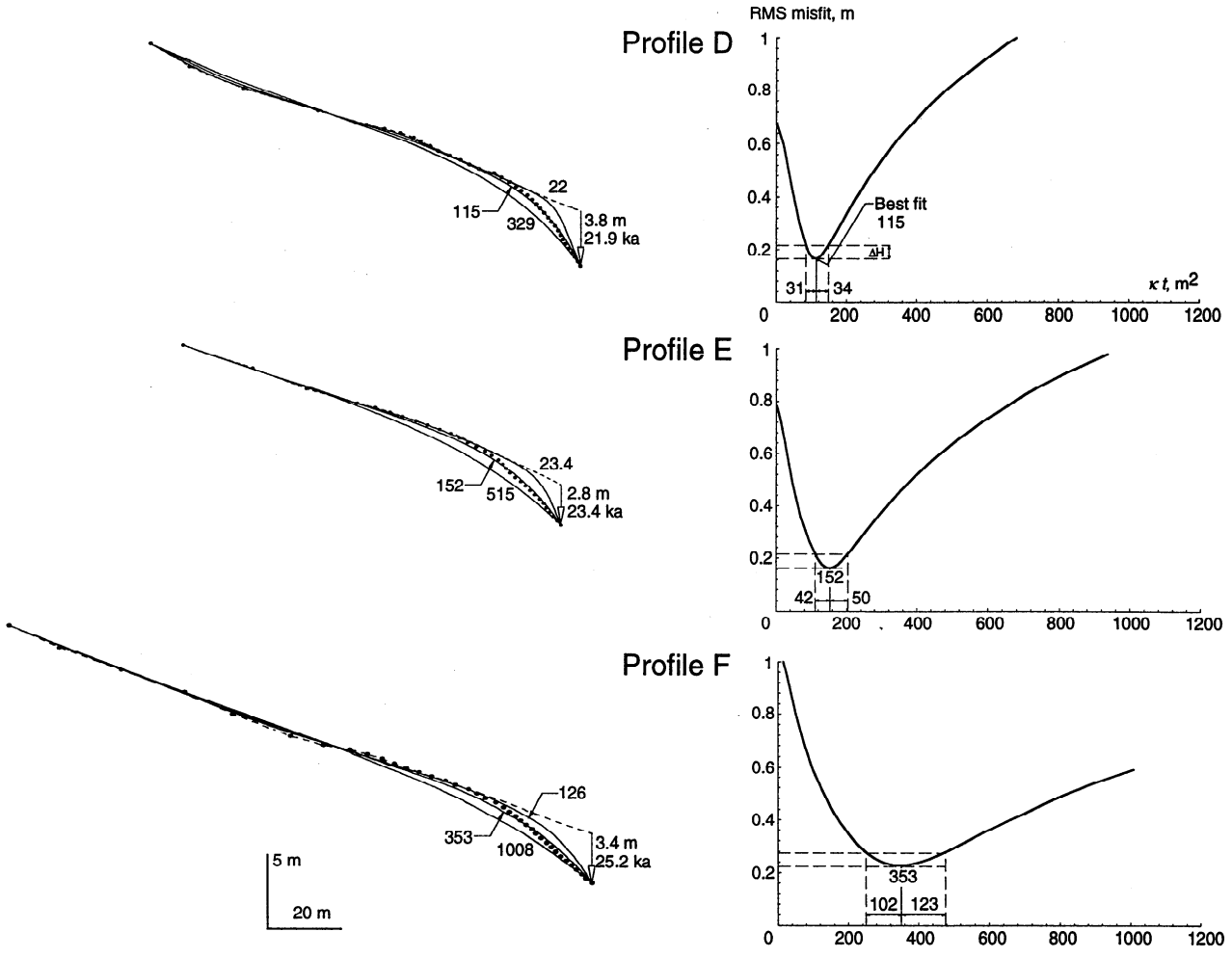

Figure 7. (continued)

is determined from the observation points (4), and thus the portion of the scarp that has been most affected by the downdropping boundary is weighted preferentially. Such weighting was implemented by *Avouac and Peltzer* [1993] and *Avouac* [1993] to enhance scarp profile analysis by permitting separate analysis of crestal and basal curvatures, minimizing the effects of irrelevant features such as small drainages and animal paths.

Best fitting κ values for the Wallace Creek scarps were determined by the forward modeling procedure described in section 4 and the appendix. Best fitting RMS values varied from 0.11 m (profile A) to 0.33 m (profile C). The analysis of profile B shown in Figure 7 is illustrative of a good fit to the tightly spaced observed topographic data near the scarp. The poor fit of profile C comes from the profile irregularities above the main portion of the scarp which require more erosion to find the minimum RMS. In general, the best fitting profiles are eroded too much in the upper portions of the scarps, and too little in the lower portions. Such an observation does not diminish the first-order acceptability of these results. Because the observed profiles have relatively sharp variations that contribute to the misfits (especially profiles C, E, and F), it is likely that they are due to secondary deformation adjacent to the SAF, rather than to variation in the transport capacity rule (i.e., nonlinear diffusion, [*Andrews and Bucknam*, 1987; *Andrews and Hanks*, 1985; *Colman*, 1987; *Hanks and Andrews*, 1989]). For all of the scarps using linear diffusion, we get a summary value of 8.6±0.8 $m^2\ kyr^{-1}$. This result is consistent within the uncertainty estimate (Table 1 and Figure 8). Note that the uncertainty in our estimate of the best fitting κ values increases with increasing distance along the scarp to the southeast (Figure 8) and morphologic age, consistent with the synthetic investigations of the model-fitting sensitivity discussed in the appendix. We also note an increase in diffusivity with inferred profile age, possibly indicating greater transport rates in the late Pleistocene. Another important result of the individual diffusivity determinations is that they do not show a dependence on scarp height in contrast to studies such as those reviewed by *Hanks and Andrews* [1989] (possibly because of a small range in height).

Table 1 provides the details of the determination of the diffusivity for Wallace Creek. For each profile, the age (and its minimum and maximum) was determined by dividing the offset distance (measured between the profile and the top of the shutter ridge, the passage of which presumably initiated exposure of the profile) by the slip rate (or its maximum or minimum). The morphologic age at the minimum RMS is listed as the best fitting age (see appendix for more discussion). The uncertainty in the morphologic age ($\pm\Delta\ \kappa t$) was conservatively determined by using the maximum uncertainty for a given profile which was always that for the increasing side of the RMS curve ($+\Delta\ \kappa t$, Figures 7 and A1). The diffusivity (κ) and its uncertainty ($\pm\Delta\ \kappa$) for each profile

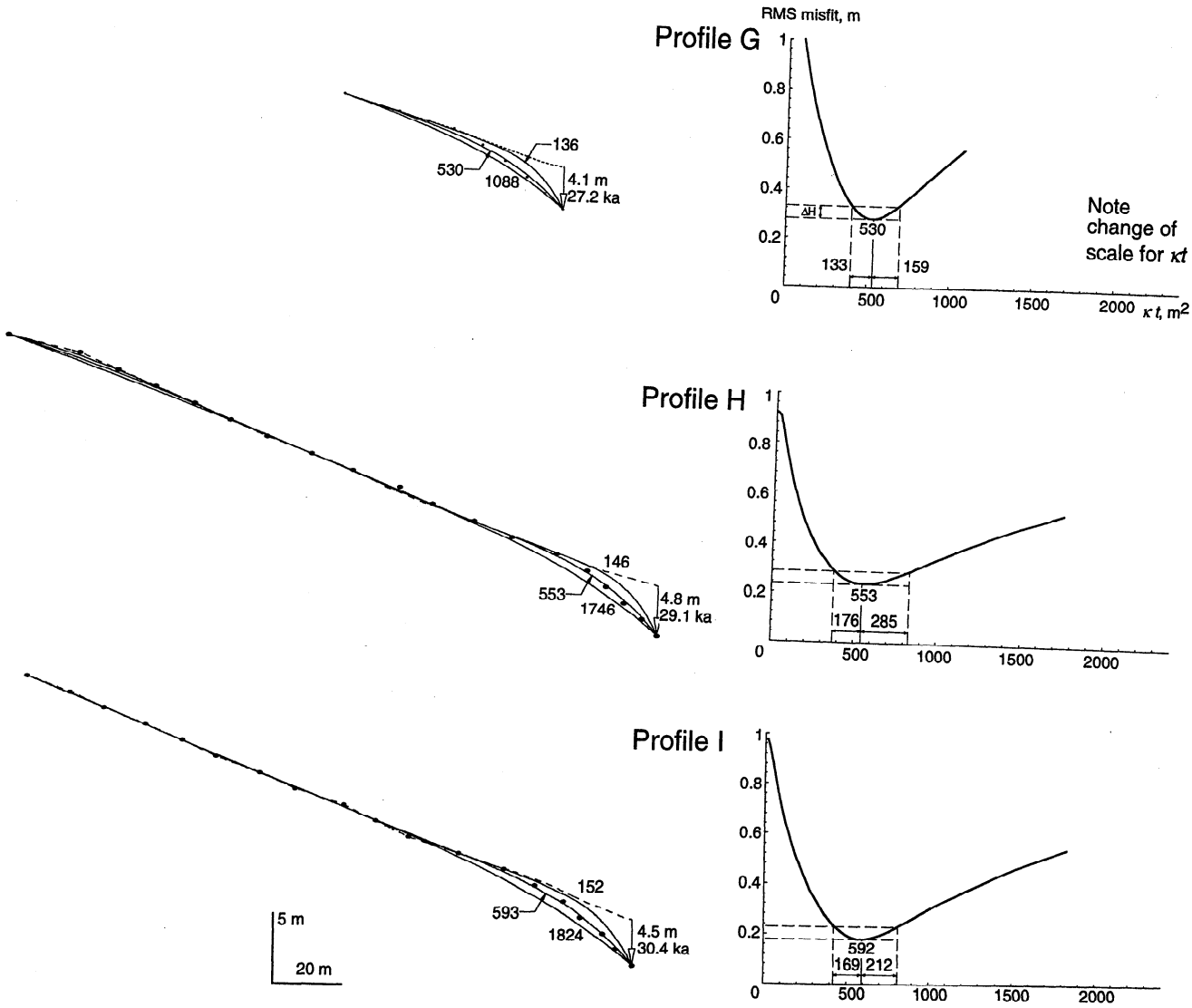

Figure 7. (continued)

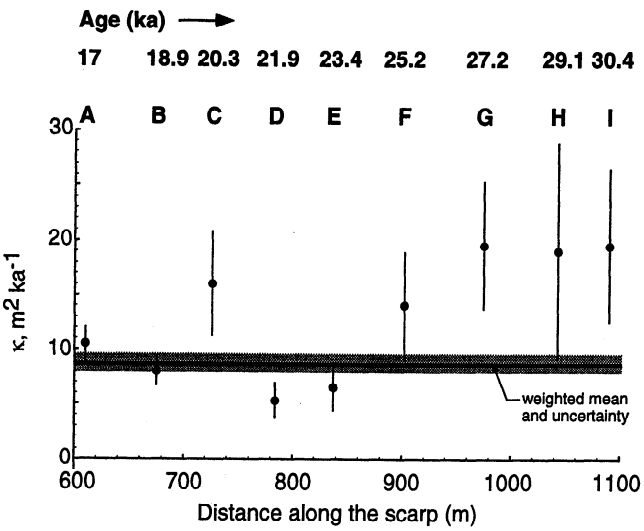

were then determined by dividing the best fitting morphologic age and its uncertainty by the age of the profile (t). The summary values were determined by applying (5) and (6).

To investigate the effect of the uncertainty in the SAF slip

Figure 8. Summary of κ values at Wallace Creek. The circle is at the mean κ value for each profile. Error bars are conservative estimates of uncertainty given an assumed 5 cm minimum misfit along the profiles (which accounts for uncertainty in the SAF slip rate). The horizontal axis is the distance along the scarp from the shutter ridge crest reference point (Figures 4 and 5), the offset of which we assume provides the lower elevation boundary control for the profiles. The locations of the profiles are shown by letters. The weighted mean of this result is 8.6 ± 0.75 m^2 kyr^{-1} (shown as the solid line and shaded bands, see Table 1).

rate (35.8+5.4/-4.1 mm yr^{-1} [*Sieh and Jahns*, 1984]), we calculated a minimum and maximum κ by dividing the morphologic age by the maximum and minimum (respectively) ages for each profile. The uncertainties in those values were determined by taking the difference between the diffusivity for the profile and the minimum and maximum diffusivities. The graphical determination of uncertainty was generally greater than that due to the variability in the SAF slip rate (varied from -0.1 m^2 kyr^{-1} (profile A) to 6.9 m^2 kyr^{-1} (profile H)). Therefore we concluded that the 5 cm criterion accounted adequately for the systematic as well as the fitting uncertainty [*Hanks*, 1997].

The choice of 5 cm as an acceptable RMS is consistent with the observation that the minimum RMS in this study and in that of *Avouac* [1993] and *Avouac and Peltzer* [1993] was about 10 cm, so we take one half of that as a measure of significance and consider it to be representative of typical misfits. *Avouac* [1993] and *Avouac and Peltzer* [1993] suggest the confidence interval of $RMS<RMS_{min}+5$ cm, saying that "Although it is not straightforward to assign a statistical meaning to the confidence interval, it provides an objective and quantitative evaluation of the precision with which the [diffusivity] is determined" [*Avouac*, 1993, p. 6750]. We concur and in order to maintain continuity between our results and theirs retain the 5 cm criterion.

8. Discussion of κ determination

Determinations of κ by other researchers in different regions have ranged from 0.1 to 16 m^2 kyr^{-1} and are summarized by *Hanks* [1997]. The lowest values of κ (0.1 m^2 kyr^{-1}) have come from lake terraces, fault scarps, and stream terraces in Israel [*Begin*, 1993; *Bowman and Gross*, 1989; *Enzel et al.*, 1995]. Morphologic dating of terrace edges, shorelines, and fault scarps in the semiarid environments of Utah, Nevada, Idaho, and Montana produced κ values of ~1 m^2 kyr^{-1} [*Hanks et al.*, 1984; *Nash*, 1984; *Pierce and Colman*, 1986]. Analysis of central Asian fault scarps produced values of diffusivity of ~5 m^2 kyr^{-1} [*Avouac and Peltzer*, 1993; *Avouac*, 1993]. Morphologic dating of marine terraces near Santa Cruz, California produced κ values of ~10 m^2 kyr^{-1} [*Hanks et al.*, 1984; *Rosenbloom and Anderson*, 1994]. The highest diffusivity reported (16 m^2 kyr^{-1}) is for the Raymond Fault scarp in southern California [*Hanks et al.*, 1984]. Initially, our Wallace Creek κ calibration results were nearly a factor of 2 greater than any previously reported κ values (they were 22.2±4.8 m^2 kyr^{-1}; [*Arrowsmith* , 1995]). Following the suggestion of T. C. Hanks (personal communication, 1995), we revised the profiles by removing the lowermost 1 m or so below a basal concavity, a portion of the profiles that is apparently within the principal surface rupture zone along the SAF so that the blocks rotate and the situation does not satisfy our assumption of constantly downdropping base level. With that modification, we achieved the better fit result reported in this paper of 8.6±0.8 m^2 kyr^{-1}. The mean diffusivity that we report has low uncertainty because of the inverse weighting by variance (see (5) and (6) and Figure 8). The individual determinations vary by a factor of 3, and we emphasize that may be more representative of the real uncertainty in the analysis.

Normal precipitation for the San Francisco Bay area is ~64 cm yr^{-1} (a minimum for Santa Cruz coast), while the central coast of California (Santa Maria) receives ~48 cm yr^{-1}, and interior central California (Bakersfield) receives ~18 cm yr^{-1}. Therefore, to judge from modern precipitation rates and assuming that the relative differences between the sites would be constant during regional climate variations of the late Quaternary and that average yearly precipitation rate is a reasonable index for material transport rates, the κ values should be greater for Santa Cruz than for the Carrizo Plain. Furthermore, the aridity of the Basin and Range and Israel suggests that transport rates should be lower than in the Carrizo Plain. This general correspondence between climate and transport rates is to be expected but should be investigated further as more determinations of diffusivity in different environments are produced. An illustrative morphological modeling investigation should test the possibility that κ has varied in time over the late Quaternary by modulating its magnitude about the mean by a climate proxy such as the $\delta^{18}O$ curve or one determined from a local paleoclimate investigation [e.g., *Fernandes*, 1994].

9. Estimation of Normal Fault Slip Rates in the Northern Elkhorn Hills

One of the primary goals when we initiated this study was to take the detailed geologic and geomorphic history determined at Wallace Creek and calibrate the geomorphic parameters to determine the slip rates along the graben-bounding normal faults in the Northern Elkhorn Hills (NEH), (Figures 2, 3, 9, and 10, summarized in Table 2) with much more easily produced field observations and topographic data. The grabens are developed about 1 km northeast of the SAF in an area of distributed deformation in the northwestern portion of the Big Bend of the SAF. There are no other data from trenching or other investigations that define the ages of these structures.

For representative profiles of the topographic maps presented in Figure 9, we assumed an initial 1° slope and slip along short normal faults provided the tectonic displacements [*Arrowsmith*, 1995; *Arrowsmith et al.*, 1996], consistent with mapping and structural geologic interpretations. The total dip slip was determined by estimating the sedimentation within the grabens and lowering of the upper ends of the profiles (simulated with zero flux boundary conditions). The morphologic dating only uses the parameter values determined for κ at Wallace Creek.

The results for morphologic dating of the grabens are acceptable for the Long and Skinny graben and the Big graben (see Table 2 and Figure 10). We assume that the diffusion age is equivalent to the time since the fault began to slip. We achieved a good fit of the Long and Skinny profile (RMS_{min} = 0.21 m). The preferred age (12.3 ± 4.1 kyr) is consistent with our expectations and with ground pattern development [*Wallace*, 1991]. The Big graben fit is fair (RMS_{min} = 0.64 m), and the age is similarly constrained (62.0 ± 10.8 kyr). Dividing the total dip slip by the summary age gives a preferred slip rate along the Long and Skinny graben fault of 1.8 mm yr^{-1} and 0.7 mm yr^{-1} for the Big graben fault (Table 2). These results are based on constant slip along the faults. The assumption of constant growth of the scarp is justified by the results of the modeling. We cannot differentiate between five and hundreds of slip events to form the scarps, but a few large slip events would not generate the same profiles as we observed, nor would slip which is not evenly distributed through the time of scarp development.

The morphologic dating of the Amphitheater normal fault was not satisfactory. This demonstrates an important result of this study: out-of-profile flow can be significant and can

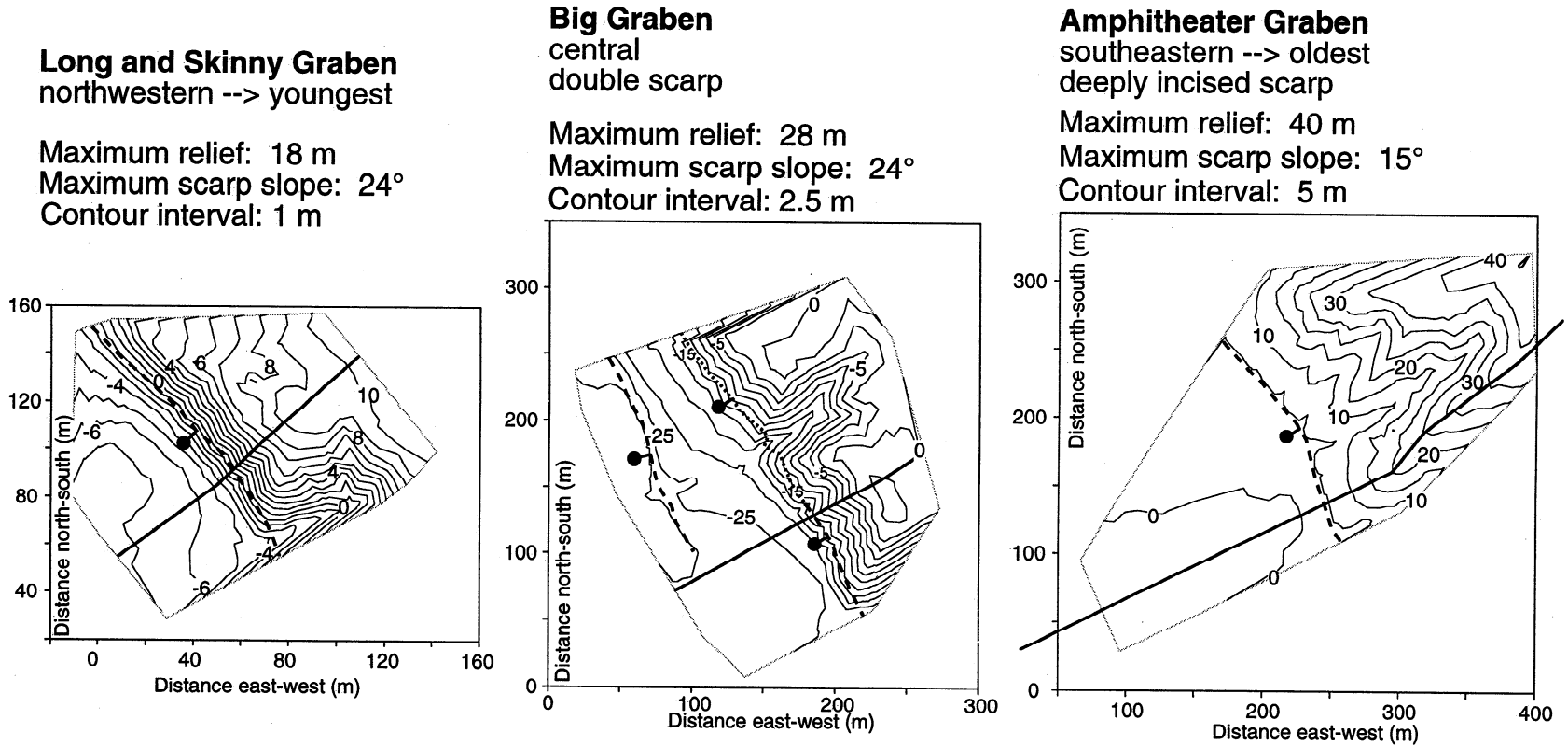

Figure 9. Comparison of Northern Elkhorn Hills (NEH) graben scarp topographic contour maps. These contour maps were made from field surveys using an electronic total station. The location of the NEH is shown in Figure 2, and the outlines of these maps are shown in Figure 3. The scarp and gully profiles investigated in the morphologic dating of this project are shown as bold lines.

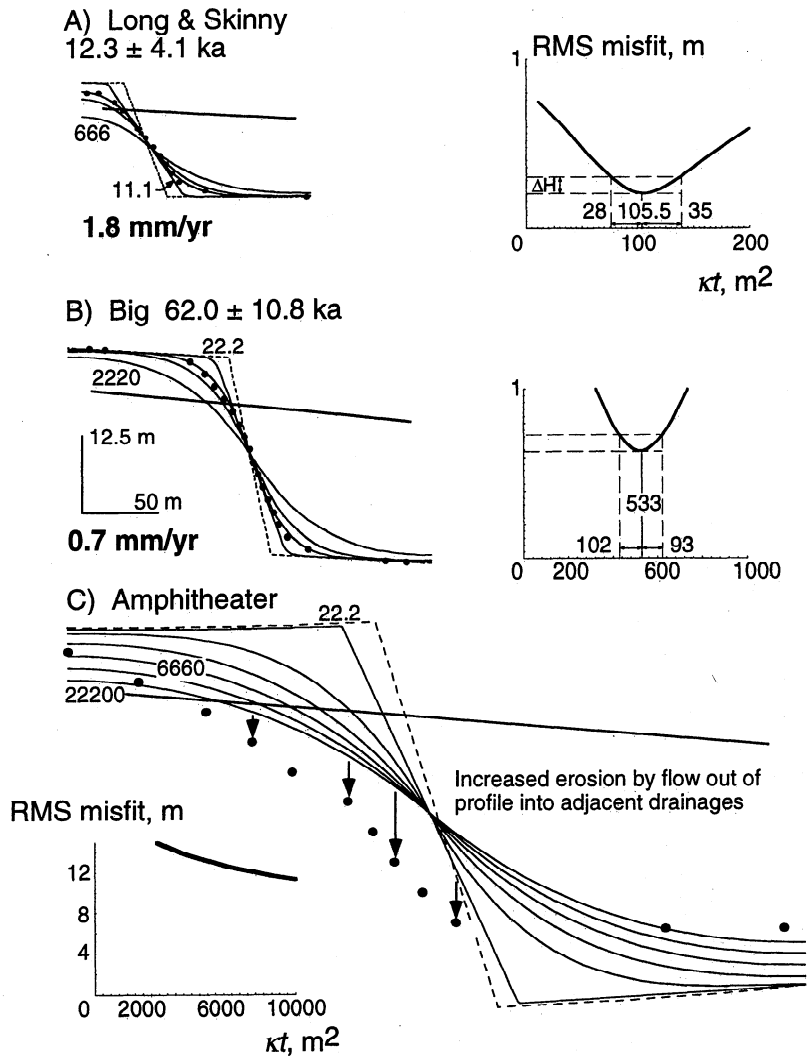

Figure 10. Morphologic dating results of NEH graben scarps. These are the scarp profiles shown in Figure 9. On the left, the initial shape is a 1° sloping surface (solid line), the final shape with no geomorphic displacements is dashed, the observations are circles, and the model profiles are solid (some are shown with corresponding κt values). The time (and its uncertainty) since the scarp began to form and the corresponding slip rate are shown. All boundary conditions are constant flux of zero (used to simulate the rounding of the upper crest and the filling of the graben). The angle of repose is 35°. Also shown are the distributions of model misfit on the right (these are explained in Figures 7 and A1; ΔH is 5 cm). The geomorphic and faulting parameters are summarized in Table 2. The apparent ages of the (a) Long and (b) Skinny and Big graben scarps are shown along with the slip rates along the faults that formed them. (c) The Amphitheater graben is not fit well because flow out of the profile increases the erosion of the upper portion of the scarp, and it is difficult to estimate the amount of graben fill and total slip.

promote increased erosion of the upper portions of scarps. The lower portion of Figure 10 shows a model result for the Amphitheater scarp. The ridge line is too low for any of our morphologic model runs. This result can be anticipated by inspection of the map in Figure 9: the scarp has been completely incised by gully development, and flow off the ridges into the drainages makes this a problem that would be best approached using a two-dimensional model [e.g., *Dietrich et al.*, 1993; *Rosenbloom and Anderson*, 1994; *Willgoose et al.*, 1991].

Morphologic dating suggests that the Big graben may be 36,000 to 66,000 years older than the Long and Skinny graben, and the summary ages indicate that they are 50 kyr apart in age. The center of the Long and Skinny graben is about 1 km northwest of the center of the Big graben. We infer that the normal faults form above reverse faults that accommodate increasing contraction adjacent to the SAF as the material enters a zone of increasing SAF-normal contraction along the Big Bend [*Arrowsmith*, 1995] (Figures 2 and 3). On the basis of their inferred ages of origin and positions, we determine that the grabens develop at a rate of about 2 cm yr^{-1}. That rate may represent the relative velocity between the material and the deformation zone associated with the Big Bend. The difference in slip rate for the two faults may indicate that the slip rates along the normal faults decrease with time as the grabens move into the Big Bend.

The stability of the Big Bend may be addressed using these results and our assumptions about the kinematic significance

Table 2. Summary of Slip Rate Determination Along Graben-Bounding Normal Faults in the Northern Elkhorn Hills

Profile	Results From Morphologic Dating						Fault Parameters				Slip Rates	
	Minimum RMS (m)	κt, m^2	$-\Delta \kappa t$, m^2	$+\Delta \kappa t$, m^2	$\pm\Delta \kappa t$, m^2	Age,[a] kyr	$\pm\Delta$ Age,[a] kyr	Fault Dip, degrees	Fault Length, m	Total Normal Dip Slip,[b] m	Fault Location at the Surface,[c] m	Preferred Slip Rate, mm yr^{-1}	Range of Possible Slip Rates, mm yr^{-1}
Long and Skinny	0.21	105.5	28	35	35	12.3	4.1	45	1000	22.25	65	1.8	1.4 - 2.7
Big	0.64	533	102	93	93	62.0	10.8	45	1000	45	85	0.7	0.61 - 0.87

[a]Age (and its uncertainty $\pm\Delta$ age) is the elapsed time since the fault began to slip and is determined by dividing the κt value by the calibrated κ of 8.6 m^2 kyr^{-1}.
[b]The total dip slip was determined by trial and error.
[c]This is distance from the divide.

of the structures. The bend may be fixed to either the southwest or northeast blocks or to neither. If it were fixed to the southwest block and we assume that the grabens develop as a consequence of secondary deformation adjacent to the leading edge of the Big Bend, we expect that the rate of development would be 3.5 cm yr^{-1}. However, if the bend (and thus the deformation zone) were fixed to the northeast block, the grabens would not develop progressively. Because the rate of development is apparently 2 cm yr^{-1}, the bend may not be fixed to either block but actually be a structural feature that develops along the SAF. Such a result is in contrast to those of *Bürgmann et al.* [1994], who showed that the bend in the SAF in the southern Santa Cruz Mountains of California apparently is fixed to the northeast block. Accordingly, structures formed there are more deeply rooted and strongly deformed relative to the material on the southwest block that moved through the deformation zone.

10. Discussion

The sources of errors in this study of morphologic dating and modeling of fault scarps in the San Andreas Fault zone are related to geometry and process. Boundary condition type (constant elevation or constant flux) is fairly easy to determine, but the amount of erosion of the upper end of the profile and amount of filling at the lower end, especially in the case of constant flux, is difficult to determine. The process types and rates are oversimplified. In particular, the mass failure algorithm and slumping to a specified angle of repose is a crude representation of the early mass failure processes of scarp erosion. The simple assumption of the process rate equation (that leads to diffusion erosion (2)) and our profile analysis method do not allow for simultaneous or variable processes along a profile in space or time.

The displacement discontinuity model for faulting allows for the displacement gradients away from the fault but assumes constant slip rate and a single rupture surface. If the recurrence interval for slip events is measured in hundreds of years and the age of the landform is measured in thousands, then the constant slip rate assumption may not be a problem. The faulting model also does not take into account the distributed fracturing and shearing commonly observed in surface ruptures [e.g., *Arrowsmith and Rhodes*, 1994]. Generally, this will tend to cause an overestimation of the morphologic age because the offset across the fault zone will not be abrupt. At least at Wallace Creek, the fault trace is apparently fairly straight, and thus we infer a minimum of distributed shear.

Most previous analyses of fault scarps have focused on the development of single or a couple-of-event scarps [e.g., *Hanks et al.*, 1984, *Nash*, 1986; *Avouac*, 1993] (although *Hanks et al.* do present a brief analysis of repeated faulting). In those analyses, the initial form is typically a steep ramp (representing the free face that has eroded to the angle of repose) in a lower slope profile (representing a faulted alluvial fan). It is important to recognize that for the analyses in this study, we assume that the continuously slipping case is representative of the long-term development of the scarps. The application of morphologic dating methods to the development of hillslopes that are driven by effectively continuous fault slip or base level change is an important contribution of this research. The number of time steps for each analysis is determined by the stability criterion of the finite difference method (directly proportional to the number

of time steps and inversely proportional to the square of the number of spatial steps). For example, the minimum number of 1028 time steps used was for the forward modeling of scarp A at a κt of 1.7 m^2. That converts to a downdrop of 7.29 mm time $step^{-1}$. At the other end of that analysis, we used 411,217 time steps for the forward modeling of scarp A at a κt of 680 m^2, resulting in 0.018 mm time $step^{-1}$ downdrop. Repeated large earthquakes along the SAF cause the offset that exposes the scarps. No creep along this portion of the SAF has been observed. A recurrence interval for the large slip events for the Carrizo segment of the SAF is about 250 years [*Sieh and Jahns*, 1984]. Given the minimum inferred age of the scarps analyzed at Wallace Creek of 17.0 kyr, that would require 68 earthquakes (or 76 mm downdrop $event^{-1}$). Analysis by *Avouac and Peltzer* [1993] indicated that the individual effects or surface ruptures on a given scarp diminish after about 10-15 events have accumulated and thus we conclude that the constant offset case is a reasonable approach. For the graben-bounding normal faults, we used a range of 1059 to 100,627 time steps, resulting in 0.447 to 40.1 mm time $step^{-1}$. In the parlance of fault scarp analysis, these are most certainly multiple event models and multiple event scarps.

The choice of a transport law (2), which invokes a linear dependence of material transport on local slope, was made to place the results of this work within the context of previous linear diffusion modeling [e.g., *Nash*, 1980; *Hanks et al.*, 1984; *Avouac*, 1993; *Hanks*, 1997]. It should be illustrative to examine modifications to the transport law as applied to these data. However, the results from the linear diffusion modeling are nearly as good as those of *Avouac and Peltzer* [1993], whose methods are similar enough to ours that we can compare the confidences of model fitting. One reason for the investigation of other transport rules was systematic misfit of profiles or apparent dependence of κ on scarp height [*Andrews and Bucknam*, 1987; *Andrews and Hanks*, 1985; *Colman*, 1987; *Hanks and Andrews*, 1989]. In this study, we have not (nor would it be easy or possibly even resolvable given the profile data density) separated the causes of misfit for model and observed profiles. The largest misfits come from relatively sharp irregularities in the scarp profiles and will not be accounted for by any reasonable change in the material transport law. The other large source of uncertainty comes from the specification of fault location and boundary condition for the graben-bounding fault analyses (Figure 10).

The investigation of morphologic development of hillslopes formed on fault scarps along the San Andreas Fault in the Carrizo Plain provides a useful method for evaluating chronologies of offset along strike-slip and normal faults. By calibrating transport rate constants using detailed information determined by trenching, we can morphologically date fault scarps and infer slip rates. The application of this analysis to the grabens is important practically (because it now is our best guess for their ages) and conceptually (because it demonstrates the application of the method).

Heuristically oriented hillslope development investigations of this type are old news to much of the geomorphic community. However, testing rules for transport capacity, determining rate constants for transport capacity, and applying these models to the development of fault scarps formed as a result of repeated strike-slip and normal-faulting slip events are new. Two developments make this contribution possible: 1) the rate constants are calibrated with the slip rate and history of landscape development at Wallace Creek that were established by paleoseismic investigations, and 2) we use a numerical landscape development model that permits arbitrary initial forms, arbitrarily oriented faults with arbitrary slip rates, and constant elevation, variable elevation, and constant flux boundary conditions. Furthermore, by quantitatively investigating the misfit between the observed final profiles and model profiles, we provide an estimate of the uncertainty in the age or rate constant and illustrate that the sensitivity of the model fitting process diminishes with increasing morphologic age.

Appendix: Best Fitting Morphologic Age and Uncertainty Determination

Figure A1 shows the dependence of RMS (4) on model morphologic age and best fitting morphologic age. For this investigation, we assumed for the initial form a ramp shape analogous to an alluvial fan with a low slope cut by a normal fault break which has slumped to the angle of repose (dashed lines in Figure A1a). Constant elevation boundary conditions are specified. The analytic solution to the diffusion erosion equation for that scenario was presented by *Hanks and Andrews* [1989]. The observed final form was determined by solving that equation for a given morphologic age and sampling it at specified intervals. The model profiles were then calculated by incrementing the morphologic age, resulting in a 0 RMS at the best fitting case. Figure A1a shows the initial observed, final observed, and model profiles for κt = 1 m^2 above and κt = 19 m^2 below. The RMS distribution is plotted in Figure A1b. The curves are steeper for morphologic ages less than the best fitting age, and they widen as the best fitting age increases as a consequence of the reduced change in elevation rate as curvature decreases with increasing profile age (consider the diffusion equation (3) which says that the change in elevation with time is proportional to the local curvature). This experiment provides an insight into determination of the best fitting profile which is most sensitive for the youngest morphologic ages of model and observed profiles because of their higher curvature.

We define confidence intervals on the best fitting value by considering all profiles that fit the observations within about 5 cm of RMS_{min} [*Avouac and Peltzer*, 1993; *Avouac*, 1993]; note the bold horizontal line in Figure A1b. The variation in morphologic age from the base of the trough to the 5 cm level provides an estimate of the model uncertainty (Figure A1b). Thus we can determine higher and lower confidence bounds on κt, and by using the larger uncertainty as the plus/minus measure of confidence on κt we provide a graphical estimate of the best fitting morphologic age with a conservative uncertainty. By considering the morphologic age range for the profiles that fit the observations within 5 cm (or any other specified value), we have incorporated the uncertainty of the known parameter ($\kappa \pm \Delta\kappa$ or $t \pm \Delta t$) in κt_{min}, and we divide by the best value of the known parameter to determine the other parameter and its uncertainty. The above description of a forward modeling procedure to determine the best fitting profile, morphologic age, and thus rate constant or age is an improvement over fitting profiles by eye. However, as suggested by the analysis leading to Figure A1, future research should focus on improving and further investigating the sensitivity of this method. The approach should be recast as a

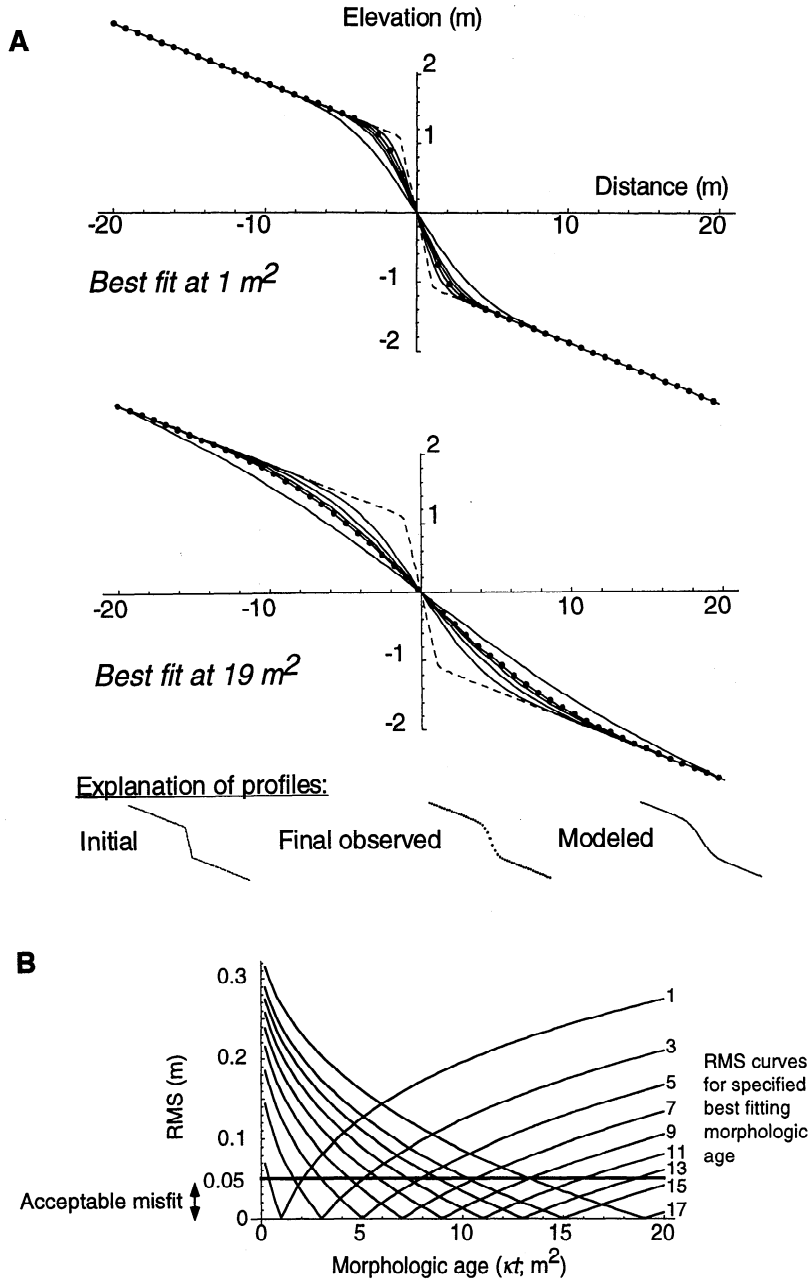

Figure A1. Investigation of root-mean-square error (RMS) dependence on morphologic age. In these examples, the final observed form is the analytic solution to the diffusion erosion equation for the ramp-shaped initial form [*Hanks and Andrews*, 1989], resulting in 0 RMS at the best fitting case. (a) Development of profiles with an initial ramp-shaped form (shown in dashes) and constant elevation boundary conditions. The model profiles (solid lines) approach, match, and develop beyond the final forms shown by circles. The upper example is for a best fitting morphologic age of 1 m^2, with model profiles of 0.5, 1, 1.5, 2, and 5 m^2. The lower example is for a best fitting morphologic age of 19 m^2, with model profiles of 5, 10, 15, 19, and 50 m^2. (b) RMS versus morphologic age for various best fitting morphologic ages (base of curve and indicated at right). The individual curves are steeper on the younger side, and they widen as the best fitting age increases as a consequence of the decreased change in elevation rate as curvature decreases with increasing profile age. The line shows the 5 cm RMS range of acceptability for profiles. The variation in morphologic age from the base of the trough to the 5 cm line provides an estimate of the model uncertainty.

formal inverse problem in order to manage parameter uncertainty more efficiently and to allow for multiple free parameters such as those that control the transport capacity rule or fault geometry, for example.

Acknowledgments. The research at Wallace Creek was first suggested by Kerry E. Sieh, and his encouragement and loan of a detailed, unpublished 1' contour interval map of the area were helpful. L.A. Rossbacher, J. Roering, and B. Yager provided valuable field assistance. Fieldwork was supported by the Stanford University Chevron Field Theses and McGee Funds, The U. S. Bureau of Land Management, and the Nature Conservancy. Discussions with R.S. Anderson, R. Bürgmann, B.P. Cohee, K.M. Cruikshank, Y. Du, S.A. Graham, T.C. Hanks, P.L. Knuepfer, K. Loague, D. Merritts, D. Montgomery, and J.D. Sims contributed to this research. We appreciate

helpful reviews of the manuscript by P.L. Knuepfer, C. Vita-Finzi, and M. Hamburger. J R. A. received support from a National Science Foundation Graduate Fellowship; the Stanford University Geological and Environmental Sciences Department, Rock Fracture Project, and Donath Fellowship; and the Stanford-U. S. Geological Survey Fellowship. Research was also supported by the U. S. Geological Survey (USGS), Department of the Interior, under USGS award 1434-94-G-2464.

References

Ahnert, F., Brief description of a comprehensive three-dimensional process-response model of landform development, *Z. Geomorphol. Suppl., 24*, 11-22, 1970.

Andrews, D.J., and R.C. Bucknam, Fitting degradation of shoreline scarps by a model with nonlinear diffusion, *J. Geophys. Res., 92*, 12,857-12,867, 1987.

Andrews, D.J., and T.C. Hanks, Scarp degraded by linear diffusion: inverse solution for age, *J. Geophys. Res., 90*, 10,193-10,208, 1985.

Arrowsmith, J R., Coupled tectonic deformation and geomorphic degradation along the San Andreas Fault System, Ph.D. dissertation, 356 pp., Stanford Univ., Stanford, Calif., 1995.

Arrowsmith, J R., and D. D. Rhodes, Original forms and initial modifications of the Galway Lake Road scarp formed along the Emerson fault during the 28 June 1992 Landers, California, earthquake, *Bull. Seismol. Soc. Am., 84*, 511-527, 1994.

Arrowsmith, J R., D. D. Pollard and D. D. Rhodes, Hillslope development in areas of active tectonics, *J. Geophys. Res., 101*, 6255-6275, 1996.

Avouac, J.-P., Analysis of scarp profiles: Evaluation of errors in morphologic dating, *J. Geophys. Res., 98*, 6745-6754, 1993.

Avouac, J.-P., and G. Peltzer, Active tectonics in southern Xinjiang, China: Analysis of terrace riser and normal fault scarp degradation along the Hotan-Qira fault system, *J. Geophys. Res., 98*, 21,773-21,807, 1993.

Begin, Z.B., Application of quantitative morphologic dating to paleo-seismicity of the northwestern Negev, Israel, *Isr. J. Earth Science, 41*, 95-103, 1993.

Bevington, P.R., and D.K. Robinson, *Data Reduction and Error Analysis for the Physical Sciences*, 2nd ed., 328 pp., McGraw-Hill, New York, 1992.

Biasi, G., and R.J. Weldon II, Quantitative refinement of ^{14}C distributions, *Quat. Res., 41*, 1-18, 1994.

Bowman, D., and T. Gross, Morphology of the latest Quaternary surface-faulting in the Gulf of Elat region, eastern Sinai, *Tectonophysics, 128*, 97-119, 1989.

Bürgmann, R., R. Arrowsmith, T.A. Dumitru, and R.J. McLaughlin, Rise and fall of the southern Santa Cruz Mountains, California, from fission tracks, geomorphology, and geodesy, *J. Geophys. Res., 99*, 20,181-20,202, 1994.

Carson, M.A., and M.J. Kirkby, *Hillslope Form and Process*, 475 pp., Cambridge Univ. Press, New York, 1972.

Colman, S.M., Limits and constraints of the diffusion equation in modeling geological processes of scarp degradation, in *Directions in Paleoseismology*, edited by A.J. Crone and E.M. Omdahl, U.S. Geol. Surv. Open File Rep., *87-0673*, 311-316, 1987.

Culling, W.E.H., Soil creep and the development of hillside slopes, *J. Geol., 71*, 127-161, 1963.

Dibblee, T.W., Regional geologic map of the San Andreas and related faults in Carrizo Plain, Temblor, Caliente, and La Panza ranges and vicinity, California, *U. S. Geol. Surv. Misc. Invest. Map, I-757*, 1973.

Dietrich, W.E., C.J. Wilson, D.R. Montgomery, and J. McKean, Analysis of erosion thresholds, channel networks, and landscape morphology using a digital terrain model, *J. Geol., 101*, 259-278, 1993.

Enzel, Y., R. Amit, N. Porat, E. Zilberman, and B.J. Harrison, Estimating the age of fault scarps in the Arava, Israel, *Tectonophysics, 253*, 305-317, 1995.

Fernandes, N.F., Hillslope evolution by diffusive processes: The problem of equilibrium and the effects of climatic and tectonic changes, Ph.D. dissertation, 145 pp., Univ. of Calif., Berkeley, Berkeley, 1994.

Galehouse, J.S., Provenance and paleocurrents of the Paso Robles formation, California, *Geol. Soc. Am. Bull., 78*, 951-978, 1967.

Hanks, T.C., The age of scarplike landforms from diffusion-equation analysis, in *Quaternary Geochronology: Applications in Quaternary Geology and Paleoseismology*, edited by J.S. Noller, J.M. Sowers, and W.R. Lettis, U.S. Nucl. Regul. Comm. Rep., NUREG/CR 5562, 1997.

Hanks, T.C., and D.J. Andrews, Effect of far-field slope on morphologic dating of scarplike landforms, *J. Geophys. Res., 94*, 565-573, 1989.

Hanks, T.C., R.C. Bucknam, K.R. Lajoie, and R.E. Wallace, Modification of wave-cut and fault-controlled landforms, *J. Geophys. Res., 89*, 5771-5790, 1984.

Hirano, M., A mathematical model of slope development: An approach to the analytical theory of erosional topography, *J. Geosci. Osaka City Univ., 11*, 13-52, 1968.

Keller, E.A., and T.K. Rockwell, Tectonic geomorphology, quaternary chronology, and paleoseismicity, in *Developments and Applications of Geomorphology*, edited by J.E. Costa, and P.J. Fleisher, pp. 203-239, Springer-Verlag, New York, 1984.

Kennie, T.J.M., and G. Petrie, *Engineering Surveying Technology*, 485 pp., John Wiley, New York, 1990.

Kirkby, M.J., Hillslope process-response models based upon the continuity equation, in *Slopes: Form and Process*, edited by D. Brunsden, *Inst. Br. Geogr. Spec. Publ., 3*, 15-30, 1971.

Kirkby, M.J., P.S. Naden, T.P. Burt, and D.P. Butcher, *Computer Simulation in Physical Geography*, 227 pp., John Wiley, New York, 1993.

McCalpin, J.P., *Paleoseismology*, 588 pp., Academic, San Diego, Calif., 1996.

Nash, D.B., Morphologic dating of degraded normal fault scarps, *J. Geol., 88*, 353-360, 1980.

Nash, D.B., Fault: A FORTRAN program for modeling the degradation of active normal fault scarps, *Comput. Geosci., 7*, 249-266, 1981.

Nash, D.B., Morphologic dating of fluvial terrace scarps and fault scarps near West Yellowstone, Montana, *Geol. Soc. Am. Bull., 95*, 1413-1424, 1984.

Nash, D.B., Morphologic dating and modeling degradation of fault scarps, in *Active Tectonics*, edited by R.E. Wallace, pp. 181-194, Nat. Acad., Washington, D. C., 1986.

Pierce, K.L., and S.M. Colman, Effect of height and orientation (microclimate) on geomorphic degradation rates and processes, late-glacial terrace scarps in central Idaho, *Geol. Soc. Am. Bull., 97*, 869-885, 1986.

Porter, S.C., Some geological implications of average Quaternary glacial conditions, *Quat. Res., 32*, 245-261, 1989.

Rosenbloom, N.A., and R.S. Anderson, Hillslope and channel evolution in the marine terraced landscape, Santa Cruz, California, *J. Geophys. Res., 99*, 14,013-14,029, 1994.

Selby, M.J., *Hillslope Materials and Processes*, 264 pp., Oxford Univ. Press, New York, 1982.

Selby, M.J., *Earth's Changing Surface*, 607 pp., Clarendon, Oxford, England, 1985.

Sieh, K.E., Slip along the San Andreas fault associated with the great 1857 earthquake, *Bull. Seismol. Soc. Am., 68*, 1421-1448, 1978.

Sieh, K.E., and R.H. Jahns, Holocene activity of the San Andreas Fault at Wallace Creek, California, *Geol. Soc. Am. Bull., 95*, 883-896, 1984.

Sieh, K.E., and R.E. Wallace, The San Andreas fault at Wallace Creek, San Luis Obispo County, California, in *Geological Society of America Centennial Field Guide--Cordilleran Section*, edited by M.L. Hill, p. 233-238, Geol. Soc. of Am., Boulder, Colo., 1987.

Smith, T.R., and F.P. Bretherton, Stability and the conservation of mass in drainage basin evolution, *Water Resour. Res., 8*, 1506-1529, 1972.

Vedder, J.G., Geologic map of the Wells Ranch and Elkhorn Hills quadrangles, San Luis Obispo and Kern counties, California, showing juxtaposed rocks along the San Andreas Fault. *U.S. Geol. Survey Misc. Invest. Map, I-585*, 1970.

Wallace, R.E., Notes on stream channels offset by the San Andreas fault, in *Proceedings of Conference on Geologic Problems of the San Andreas Fault*, edited by W.R. Dickinson and A. Grantz, pp. 6-21, Stanford Univ. Publ. in the Geol. Sci., Stanford, Calif., 1968.

Wallace, R.E., The San Andreas fault in the Carrizo Plain--Temblor Range region, California, in *The San Andreas fault in southern California*, edited by J.C. Crowell, Spec. Publ. Calif. Div. Mines Geol., 118, p. 241-250, 1975.

Wallace, R.E., Degradation of the Hebgen Lake fault scarps of 1959, *Geology, 8*, 225-229, 1980.

Wallace, R.E., *The San Andreas Fault System, California*, 283 pp., U.S. Geol. Surv. Prof. Pap., 1515, 1990.

Wallace, R.E., Ground-squirrel mounds and related patterned ground along the San Andreas Fault in central California, U.S. Geol. Surv. Open File Rep., *91-0149*, 1991.

Wallace, R.E., and S.S. Schulz, Aerial views in color of the San Andreas fault, California, U.S. Geol. Surv. Open File Rep., *83-0098*, 1983.

Welty, J.R., C.E. Wicks and R.E. Wilson, *Fundamentals of Momentum, Heat, and Mass Transfer*, 803 pp., John Wiley, New York, 1984.

Willgoose, G., R.L. Bras, and I. Rodriguez-Iturbe, A coupled channel network growth and hillslope evolution model, 1, Theory, *Water Resour. Res., 27*, 1671-1684, 1991.

Worsley, P., Radiocarbon dating: Principles, application, and sample collection, in *Geomorphological Techniques*, edited by A.S. Goudie, pp. 383-393, Unwin Hyman, Boston, Mass., 1990.

Yeats, R.S., Historical paleoseismology, in *Proceedings of the Workshop on Paleoseismology*, edited by C.S. Prentice, D.P. Schwartz, and R.S. Yeats, U.S. Geol. Surv. Open File Rep., *94-0568*, 208-210, 1994.

Yeats, R.S., K.E. Sieh, and C.R. Allen, *The Geology of Earthquakes*, 576 pp., Oxford Univ. Press, New York, 1997.

J R. Arrowsmith, Department of Geology, Arizona State University, Tempe AZ 85287-1404. (e-mail: ramon.arrowsmith@asu.edu)

D.D. Pollard, Department of Geological and Environmental Sciences, Stanford University, Stanford, CA 94305-2115. (e-mail: dpollard@pangea.stanford.edu)

D.D. Rhodes, Department of Geology, Whittier College, Whittier, CA 90608. (e-mail: drhodes@whittier.edu)

(Received January 17, 1997; revised December 18, 1997; accepted January 21, 1998.)